Available online at www.sciencedirect.com

ScienceDirect

IFAC Papers Online CONFERENCE PAPER ARCHIVE

IFAC PapersOnLine 52-15 (2019) 364–369

Modelling, Validation and Control of DELIAN Flexible Manipulator

Fabio Comi[1], Aitor Orive Miguel[1], Francesco Cavenago[2], Gianni Ferretti[1], Gianantonio Magnani[1], Andrea Rusconi[3]

[1] *Dipartimento di Elettronica, Informazione e Bioingegneria, Politecnico di Milano, Piazza Leonardo da Vinci 32, 20133 Milano, Italy*

[2] *Dipartimento di Scienze e Tecnologie Aerospaziali, via La Masa 34, 20156, Milano, Italy (e-mail: {fabio1.comi, aitor.orive, francesco.cavenago, gianni.ferretti, gianantonio.magnani}@polimi.it)*

[3] *Leonardo SpA, Viale Europa, 20014, Nerviano (MI), Italy (e-mail: andrea.rusconi@leonardocompany.it)*

Abstract: This paper deals with the modelling, validation and control of the ESA space manipulator DELIAN. A numerical model accounting for joints and links flexibility is developed, and structural parameters are identified through experiments on the real robot. Then, the model is validated comparing the behavior of the simulated system with the real one. Moreover, an analysis aiming to understand the contribution of each elastic element to the overall flexibility is carried out. Finally, wave-based control technique is combined to the well-known P/PI scheme in order to reduce system vibrations. Especially, a velocity-based implementation of the WBC is introduced which provides superior performance with respect to the position-based one.

Keywords: Space robotics, Flexible arms, Modelling, Parameter identification, Least-squares identification, Validation, Sensitivity analysis, Wave-Based control.

1. INTRODUCTION

In the last decades, the number of missions aiming to the space exploration has been growing significantly. In particular, the study of the Martian environment has become of primary interest after the recent discovery of liquid water on the planet. In this context, ESA Mars Robotic Exploration Preparation (MREP) Programme proposes a Technology Development Plan (TDP) identifying key enabling technologies to be developed within Europe to support ongoing and future planetary missions. DELIAN (DExterous LIghtweight Arm for exploratioN) project (Rusconi et al. (2015)), belonging to the theme on robotics and rover technologies of the MREP TDP, aims at developing a general purpose lightweight robotic arm, a device to enable accessibility to the Martian surface for sample acquisition, sample retrieval or instrument deployment, as part of a rover or a lander platform.

The choice of an ultra-lightweight manipulator leads to several benefits in terms of energy consumption, operational speed, payload-to-manipulator weight ratio and overall mission cost. On the other hand, these manipulators are characterized by the low structural stiffness of the links and joints, introducing vibrations which affect the positioning accuracy of the end-effector. Accurate flexible model are required in order to analyze these complex multibody systems and design efficient controllers.

This paper presents the development of an accurate flexible model of DELIAN, exploiting an object oriented procedure (Bascetta et al. (2017)) for the introduction of links flexibility and the two mass approximation (Spong (1987)) for the modelling of the elastic joints. The structural parameters are identified by a sequence of experimental tests performed on the manipulator, while the validation of the model is obtained by comparing the behaviour of the real system to the simulated one in different scenarios. A sensitivity analysis is performed in order to evaluate which flexible element, i.e. joints and links, most affects the first antiresonance/resonance pair, limiting the control bandwidth. It turns out that the elasticity of the two links is much more critical, confirming the importance of including their flexibility in the model.

As regards the control, many authors addressed the problem of reducing the oscillation in flexible manipulators investigating different strategies, such as model-based approaches (De Luca et al. (1989)), adaptive control (Yang et al. (1992)), H_∞ control (Farruggio and Menini (2000)), integral resonant control (Pereira et al. (2010)). In this paper, the wave-based control (WBC) strategy, proposed in O'Connor et al. (2009), is adopted, first, inside the position loop and, then, inside the velocity loop of the P/PI joint controller to damp the oscillations of the robot. It is shown that the latter solution provides superior performance, improving significantly the positioning of the end-effector. Differently to Malzahn and Bertram (2016), where a similar idea is presented, no strain gauges are used and the reference signals are modulated using the measurements of the encoders mounted on the motor and link side of the joints.

The paper is organized as follows. In Section 2, an overall description of DELIAN is given. Section 3 deals with the development of the numerical model of DELIAN including both the links and joints flexibility. In Section 4, the identification of the structural parameters of the model is

10.1016/j.ifacol.2019.11.702

carried out, while Section 5 describes the process applied to validate the model. Finally, Section 6 discusses the effectiveness of the wave-based approach for the joint control to reduce vibrations and in Section 7 the main conclusions are drawn.

2. DELIAN OVERVIEW

DELIAN is a 6 degrees of freedom (DoF) robotic arm. Two joints are placed on the shoulder, two on the elbow and the last two on the wrist. The architecture of each joint consists of a Maxon brushed DC motor, equipped with a motor position sensor characterized by a resolution which ranges from 16 to 500 count/rev. The transmission is characterized by a double reduction stage consisting of a planetary gear on the first stage and a harmonic drive in series on the second stage, which leads to an extremely high gear ratio, ranging from 21750 to 44340. This choice was made in order to minimize the mass to torque ratio (Rusconi et al. (2015)). An accurate Anisotropic Magneto Resistive (AMR) angular position sensor, providing a resolution of 0.001° and an accuracy of ±0.003°, has been integrated directly at the link side of each joint. The joint has been designed and manufactured to operate on Mars or Moon environment with a temperature range from -55C to +60C.

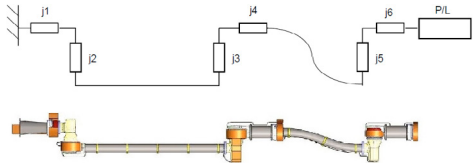

Fig. 1. DELIAN configuration.

The material selected for the links is an alloy of aluminum, as it has a good strength to weight ratio with a nominal Young's modulus equal to 78 GPa. A representation of the arm is reported in Fig. 1.
Finally, DELIAN end-effector is equipped with a distance sensor, mounted mainly for calibration purpose, and a force sensor.

3. DELIAN FLEXIBLE MODEL

3.1 Links flexibility modelling

In order to address the problem of modelling the link flexibility, the object-oriented modelling approach to general flexible multibody systems, described in Bascetta et al. (2017), is here adopted. For the sake of brevity, just a brief description of the procedure is reported in the following.

The approach has been mainly addressed according to this conceptual scheme:

1) A Floating Frame of Reference (FFR) is attached to each link, and the position $\bar{\boldsymbol{u}}$ of a point along the link is described as the superposition of an undeformed position vector $\bar{\boldsymbol{u}}_0$ and a local flexible deformation contribution $\bar{\boldsymbol{u}}_f$, both defined with respect to the FFR. Therefore,

$$\bar{\boldsymbol{u}} = \bar{\boldsymbol{u}}_0 + \bar{\boldsymbol{u}}_f \tag{1}$$

2) Assuming small deformations and a linear elasticity, the flexible deformation can be approximated by a functional basis space with finite dimension, say M, so that the vector $\bar{\boldsymbol{u}}_f$ can be expressed by the finite dimensional product

$$\bar{\boldsymbol{u}}_f = \boldsymbol{S}\boldsymbol{\xi} \tag{2}$$

where $\boldsymbol{S}$ is the $[3 \times M]$ shape functions matrix (i.e., a matrix of functions defined over the body domain and used as a basis to describe the deformation field of the body itself) and $\boldsymbol{\xi}$ is the M-dimensional vector of deformation degrees of freedom, or modal coordinates.

3) The equations of motion for the single flexible body are derived in the FFR applying the principle of virtual work. The resulting mass matrix depends on some inertia invariants, related to the shape functions and to the body mass distribution.

Solid modelling CAD packages can be conveniently used for the off-line computation of the parameters characterizing the flexible link dynamics, especially in the case of complex geometries, performing also an orthonormalization of mode shapes, which is of great importance for model simplification. Indeed, in the DELIAN case, the model of each flexible link is first preprocessed through the Abaqus suite and then the data describing the dynamic model of the flexible link are imported into the Modelica/Dymola environment. Finally, the blocks of the flexible links models are generated and integrated with the model of the transmission chain. A more comprehensive argumentation can be found in Ferretti et al. (2014).

3.2 Joint linear model

A two mass system is introduced to model each joint (Spong (1987)) and is reported in Fig. 2, where:

- $J_{motor} = J_m + J_{pl}$
- $J_{load} = J_l + J_{hd}{n_{hd}}^2$
- $K_{eq} = \frac{K_{pl}K_{hd}}{K_{hd}+K_{pl}{n_{pl}}^2}$
- $D_{eq} = \frac{K_{hd}D_{pl}+K_{pl}D_{hd}}{K_{hd}+K_{pl}{n_{pl}}^2}$

with $J_{pl}, K_{pl}, D_{pl}, n_{pl}$ and $J_{hd}, K_{hd}, D_{hd}, n_{hd}$ the inertia, stiffness, damping coefficient and gear ratio of the planetary gearbox and harmonic drive, respectively, and J_m and J_l the motor and load inertia, respectively. In order

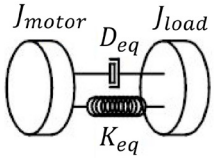

Fig. 2. Two mass system.

to describe the friction acting on the joint, the classical discontinuous friction model is used. The model takes into account the static friction τ_s, the Coulomb friction τ_c and the viscous coefficient D_m. The friction torque τ_{fr} can be computed as

$$\tau_{fr} = D_m\dot{q}_m + \tau_c \text{sign}(\dot{q}_m) \quad \text{for} \quad \dot{q}_m \neq 0 \tag{3}$$

with the condition

$$\tau_{fr} \leq \tau_s \quad \text{for} \quad \dot{q}_m = 0 \tag{4}$$

where $\dot{q}_m$ is the motor velocity.

4. PARAMETERS IDENTIFICATION AND MODEL VALIDATION

Most of the manipulator parameters included in the developed model are not initially available. The identification and validation of such parameters are particularly important since their values can modify the model behaviour significantly. The unknown parameters necessary to characterize the joint model are the stiffness and damping of the equivalent reduction stage (K_{eq}, D_{eq}) and the friction coefficients (τ_s, τ_c, D_m). Also, the identification of the Young's modulus for both the links is performed in order to include the effects of their flexibility in the model.

4.1 K_{eq}, D_{eq}, τ_c, D_m identification

Generally, the joint friction and transmission parameters can be identified separately. For the friction, the motor velocity steady state response is usually used, while impulsive tests are performed to evaluate the transmission stiffness and damping. In the case of DELIAN, it has been observed that the supplied current, in steady state condition, is extremely low and consequently its measurement is not reliable. Moreover, it is impossible to perform impulsive tests directly on the fully assembled structure. These issues led to the choice of identifying all the parameters together through a Least-Square approach, exploiting the transient response, which is characterized by higher current values. During the transient, the dynamic equation of the motor is

$$J_m \ddot{q}_m = \tau_m - \tau_{lm} - \tau_{fr} \tag{5}$$

where

- $\tau_m = K_t I$ is the motor torque
- $\tau_{lm} = K_{eq}(q_m - n q_l) + D_{eq}(\dot{q}_m - n\dot{q}_l)$ is the transmission torque

with K_t the torque constant, q_m and q_l the motor and load angular displacement and $n_{eq} = n_{pl} \cdot n_{hd}$.
Therefore, Eq. (5) can be written as

$$K_t I - J_m \ddot{q}_m = K_{eq}(q_m - n_{eq} q_l) + D_{eq}(\dot{q}_m - n_{eq}\dot{q}_l) + \tau_c + D_m \dot{q}_m \tag{6}$$

In Eq. (6) all the parameters are included. Exciting the system with different current values (at least 4), having the measurements of q_m, q_l, and obtaining $\dot{q}_m$, $\ddot{q}_m$, $\dot{q}_l$ through numerical differentiation, the Least-Square method is applied for the estimation of the unknown parameters. The resulting set of n equations can be written as follows

$$\boldsymbol{y} = \boldsymbol{X}\boldsymbol{\mu}, \tag{7}$$

with

$$\boldsymbol{y} = \begin{bmatrix} K_t I_1 & -J_m \ddot{q}_{m_1} \\ K_t I_2 & -J_m \ddot{q}_{m_2} \\ \vdots & \vdots \\ K_t I_n & -J_m \ddot{q}_{m_n} \end{bmatrix},$$

$$\boldsymbol{X} = \begin{bmatrix} (q_{m_1} - n_{eq} q_{l_1}) & (\dot{q}_{m_1} - n_{eq}\dot{q}_{l_1}) & 1 & \dot{q}_{m_1} \\ (q_{m_2} - n_{eq} q_{l_2}) & (\dot{q}_{m_2} - n_{eq}\dot{q}_{l_2}) & 1 & \dot{q}_{m_2} \\ \vdots & \vdots & \vdots & \vdots \\ (q_{m_n} - n_{eq} q_{l_n}) & (\dot{q}_{m_n} - n_{eq}\dot{q}_{l_n}) & 1 & \dot{q}_{m_n} \end{bmatrix}, \boldsymbol{\mu} = \begin{bmatrix} K_{eq} \\ D_{eq} \\ \tau_c \\ D_m \end{bmatrix}.$$

The Least-Squares solution to the problem is a vector $\hat{\boldsymbol{\mu}}$ which estimates the unknown vector of coefficients $\boldsymbol{\mu}$:

$$\hat{\boldsymbol{\mu}} = (\boldsymbol{X}^T \boldsymbol{X})^{-1} \boldsymbol{X}^T \boldsymbol{y}. \tag{8}$$

Concerning the first three joints, the identified parameters are reported in Tab. 1.

Table 1. Identified joint parameters.

	Joint 1	**Joint 2**	**Joint 3**
K_{eq} [Nm/rad]	$3.07 \cdot 10^{-5}$	$2.2 \cdot 10^{-5}$	$2.96 \cdot 10^{-5}$
D_{eq} [Nms/rad]	$8.07 \cdot 10^{-8}$	$3.18 \cdot 10^{-8}$	$8.35 \cdot 10^{-8}$
τ_c [Nm]	$7.37 \cdot 10^{-5}$	$1.2 \cdot 10^{-4}$	$7.73 \cdot 10^{-5}$
D_m [Nms/rad]	$7.2 \cdot 10^{-8}$	$2.5 \cdot 10^{-8}$	$6.93 \cdot 10^{-8}$

4.2 τ_s identification

In order to identify the static friction, the current supplied to the motor is increased slowly until the motor starts moving. Once the current I_s is identified, τ_s is determined as $\tau_s = K_t I_s$. The results of the identification are reported in Tab. 2. Examining each joint, it has been noted that

Table 2. Static friction.

	Joint 1	**Joint 2**	**Joint 3**
τ_s [Nm]	$2.99 \cdot 10^{-4}$	$2.6 \cdot 10^{-4}$	$2.45 \cdot 10^{-4}$

the unusually high $\frac{\tau_s}{\tau_c}$ ratio is related to the extremely high values of transmission gear ratio and increases as n_{eq} increases.

4.3 Young's modulus identification

Two experiments are designed to estimate the Young's modulus of the links. Since the manipulator is fully assembled, and thus single link cannot be isolated, strategic configurations of DELIAN (see Fig. 3) are chosen enabling the estimation of Young's moduli through a static deflection analysis. Indeed, in these configurations, the single link can be modeled as a cantilever beam with a lumped mass at the free end.

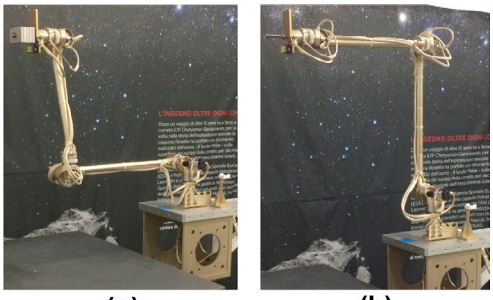

Fig. 3. Configuration of first (a) and second (b) experiment. Courtesy of Leonardo Spa and European Space Agency.

The tip deflection d can be computed as

$$d = \frac{1}{3}\frac{FL^3}{EJ} \tag{9}$$

where F, L, E, J are the weight of the lumped mass, the equivalent length of the beam, the Young's modulus and the area moment of inertia, respectively. Then, the Young's modulus can be isolated from Eq. (9).

In each experiment, two load conditions are considered. In the first one, the end-effector is unloaded, while in the other one, some known loading masses are added. Then, from Eq. (9) the Young's modulus for each link can be computed. Indeed, F can be evaluated knowing the loading masses, L and J are known from the CAD models of the links and the deflection d is computed exploiting the measured position of the end-effector and the knowledge of the robot geometry. Note that the joint flexibility is compensated by the joint controller. Indeed, in the experiments, each joint is controlled by a P/PI controller, where an inner PI controller is closed on the motor velocity, while an outer proportional controller is closed on the load position.

Tab. 3 reports the results of the identification, including the percentage difference from the nominal value.

Table 3. Young's modulus results.

	Young's modulus	**From nominal**
Link 1	93.47 GPa	+19.83%
Link 2	87.23 GPa	+12.05%

The difference from the nominal value is not completely unexpected. In fact, the quantities coming from the experimental identification are affected by the rigidity of the flanges used to connect joints and links. This results in an increasing of the equivalent stiffness of the links with respect to the case in which they are unconstrained.

4.4 Model validation

In order to assess the reliability of the numerical model, several experimental tests have been carried out on DELIAN. For each joint, two sets of closed-loop experiments have been performed. The first one evaluates the motor and load angular velocity responses to a step on the motor velocity reference, while the second test evaluates the motor and load position responses to a step on the load position reference. In the first test only PI velocity controller is closed on the motor velocity, while in the second one the P/PI controller is used. For the sake of brevity, the validation process is reported only for the second joint; however, similar results have been obtained for the other joints.

In Fig. 4 the motor angular velocity response of the real system is compared with the response of the simulated system. The model response properly represents the real system behaviour. Comparing the settling time and steady state value, the results are satisfactory.

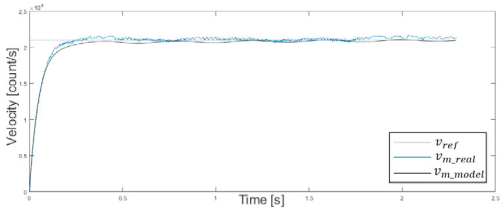

Fig. 4. Motor angular velocity response comparison.

Fig. 5 reports the comparison between the load angular velocity response in the real and simulated robot. The load response is affected by oscillations due to both joints and links flexibility. It can be noted that the real system behavior is accurately reproduced by the model, especially the first resonance contribution. In the simulation, the second mode is also clearly visible, while it is not in the real response due to high frequency disturbances.

Regarding the position closed-loop experiment, the comparison between the real and the simulated responses of the motor and load angular position is shown in Fig. 6 and Fig. 7, respectively. As it can be seen from the two comparisons, the model follows the behavior of the real system satisfactorily.

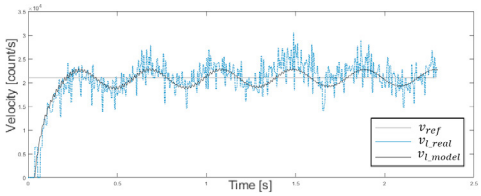

Fig. 5. Load angular velocity response comparison.

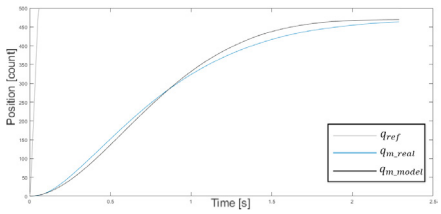

Fig. 6. Motor angular position response comparison.

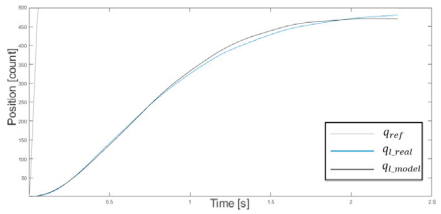

Fig. 7. Load angular position response comparison.

5. COMPONENTS ELASTICITY ANALYSIS

5.1 Static deflection analysis

It is interesting from a structural point of view to study how the different elastic components contribute to the whole system flexibility. However, it is not trivial to perform such a comparison between elements of different nature, i.e. links and joints. A possible way is proposed in Magnani and Rocco (2010), and involves the approximation of each elastic element to an equivalent torsional spring, with the aim of comparing the deformation coming from each component.

Then, the deformation can be expressed as an angular displacement $\Delta\Theta_i$, which can be measured from the validated model. To obtain deformations, the manipulator is controlled to keep a configuration in which the gravity plays a significant role (Fig. 8).

The resulting deformations are reported in Tab. 4 The link flexibility turns out to be the principal source of deformation of the system. In particular, the second link, which

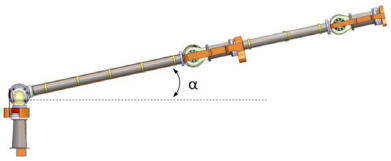

Fig. 8. Manipulator chosen posture.

Table 4. Deformation of each elastic element.

$[\alpha = 45°]$	**Link 1**	**Link 2**	**Joint 2**	**Joint 3**	**Joint 5**
$\Delta\Theta$	0.49°	1.09°	0.17°	0.08°	0.02°

presents the lower Young's modulus, leads to the largest deformation. This analysis has a significant importance since it suggests on which component it is more convenient to apply structural correction to achieve higher accuracy performances.

5.2 Sensitivity analysis

Another way to compare the relative contribution of each flexible component to the overall vibration of the manipulator is to perform a sensitivity analysis. Since it is well known that the first resonance is the most critical for the control design, the stiffness of each elastic element is increased one by one and then the effects on the first mode pulsation are evaluated. Tab. 5 reports the simulation results, obtained by the spectral analysis.

Table 5. Sensitivity analysis results.

	Scenario	**Increment**	ω_n **Variation**
(A)	Nominal	-	-
(B)	$K_{eq_2} \uparrow$	+20%	+2.2%
(C)	$K_{eq_3} \uparrow$	+20%	+1.7%
(D)	$K_{eq_5} \uparrow$	+20%	+0.7%
(E)	$E_1 \uparrow$	+20%	+7.9%
(F)	$E_2 \uparrow$	+20%	+4.6%

The results highlight how the system is more sensitive to links elasticity variation rather than the joints one. It can be clearly noted that a variation of the Young's modulus of the first link, the longest one, leads to higher variation of the first mode natural frequency.

6. JOINT CONTROL

DELIAN joints are controlled through the classical P/PI controller, namely a cascade controller with an inner loop on the motor velocity and an outer loop on the load position. A detailed analysis of the control design and related issues deriving from the peculiar features of DELIAN is presented in Cavenago et al. (2017). In the following, the use of the wave-based control inside the P/PI architecture is proposed in order to reduce the load vibrations. In Malzahn and Bertram (2016), the wave-based control is implemented on a 3DoF flexible robotic arm. Especially, the authors show that an active oscillation damping action can be introduced modulating either the amplifier input voltage, or the motor velocity controller, or the motor position controller. In all the cases, they use measurements from the motor encoder and some strain gauges fixed to the links. In this paper, the oscillation damping is introduced modulating, first, the link-side joint position and then the motor velocity. In both cases, no strain gauges are used. Indeed, the modulation is done exploiting the measurements from the encoders mounted on the motor and link side. The two strategies are compared and the superior performance of the latter one is shown.

6.1 Wave-based control

Before proceeding, it is pointed out that detailed derivation of the WBC is beyond the scope of this paper, and thus only a short introduction of the technique is given. A more comprehensive discussion can be found in O'Connor et al. (2009).

The idea behind the WBC is to consider the real motion of any points of the system as a summation of a launch wave and a return wave. Indeed, when the actuator moves, it launches a wave (*launching wave* a_n) into the system. Then, due to the flexibility of the system, also another wave (*returning wave* b_n) can be identified, which passes through the system and it is reflected to arrive back at the actuator. Therefore, a wave-based controller can be designed to follow a desired trajectory and at the same time to absorb the return wave. The actuator launches a desired displacement wave into the system while acting as an active vibration damper.

Considering the isolated joint-link flexible system, it can be modelled as a lumped system made up of masses and springs. The motion of each mass is the summation of the launching and returning wave (see Fig. 9).

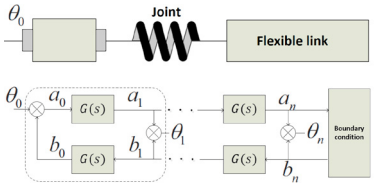

Fig. 9. Wave-Based control scheme.

In the case of DELIAN, θ_0 is the displacement of the motor and θ_1 is the displacement of the joint load. $G(s)$ is the wave transfer function (WTF) which is the transfer function between the motion of any mass and that of the next mass. For control purposes, this function can be approximated as a 2^{nd} order function as

$$G(s) \approx \frac{\omega_n^2}{s^2 + s\omega_n + \omega_n^2} \tag{10}$$

where ω_n is the natural frequency of the mass-spring system. In order to achieve trajectory tracking and vibration absorption, the control input should be

$$\theta_0(t) = \frac{1}{2}\theta_{ref}(t) + b_0(t) \tag{11}$$

where $\theta_{ref}(t)$ is the position reference and $b_0(t)$ is the returning wave at the actuator interface. The resulting control structure is reported in Fig. 10.

It is worth highlighting that ω_n changes depending on the configuration of the manipulator. An adaptive wave-based control accounting for the variation of the natural frequency ω_n would increase the control effectiveness.

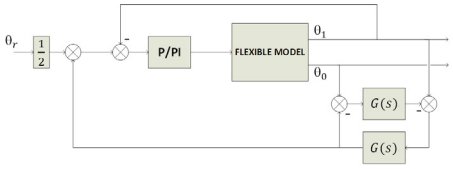

Fig. 10. Classical Wave-Based implementation.

6.2 Velocity wave-based control

Since it has been noted that the WBC on the joint load position provides poor performance in terms of settling time and steady state error, the control structure previously presented is slightly modified. The WBC is applied to the inner velocity control loop, considering velocity waves instead of displacement waves. This choice is motivated by the fact that the velocity controller is required to regulate faster dynamics, and thus the active vibration damper should act at this level. On the other hand, the outer position loop is exploited to achieve the required steady state and low frequency accuracy. The final structure is reported in Fig. 11.

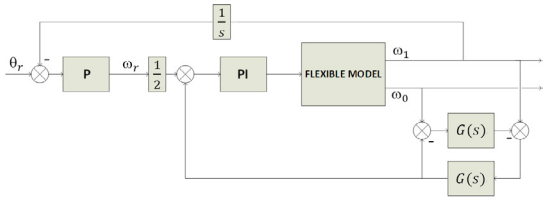

Fig. 11. Velocity Wave-Based implementation.

A comparison between the two WBC implementations is reported in Fig. 12. Thanks to the velocity WBC (VWBC), the end-effector moves precisely to the target, with slight vibrations, rapid settling time and no steady-state error comparing with the classical WBC. The end-effector vibration reduction achieved by the WBC and the VWBC is 71.9% and 83.1%, respectively.

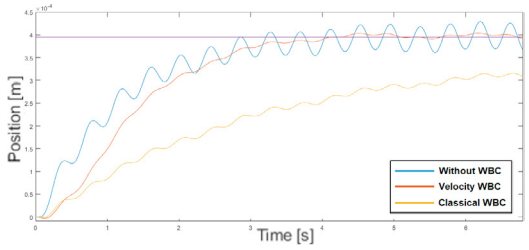

Fig. 12. X-positioning of the end-effector.

The results show the substantial benefits in oscillation reduction introduced by the WBC with respect to the standard P/PI control technique. Especially, the VWBC implementation introduced in this paper turns out to further improve the performance of the classical WBC configuration allowing higher positioning accuracy of the end-effector.

7. CONCLUSIONS

Modelling, validation and control of DELIAN flexible manipulator have been presented in this paper. The system has been modeled by means of an object-oriented modelling approach and structural parameters have been identified through experimental tests. Afterwards, it has been shown that model can represents the real robot behavior accurately. The significant role of links flexibility in determining the first antiresonance/resonance pair of the manipulator has been demonstrated. Finally, the use of the velocity wave-based control inside the P/PI architecture has been proposed to improve positioning accuracy.
Future works will focus on the stability analysis of the proposed controller and its implementation on real hardware. Afterwards, an adaptive scheme to account for the variation of the natural frequency in $G(s)$ will be investigated.

REFERENCES

Bascetta, L., Ferretti, G., and Scaglioni, B. (2017). Closed form Newton-Euler dynamic model of flexible manipulators. *Robotica*, 35(5), 1006–1030.

Cavenago, F., Bascetta, L., Magnani, G., and Rusconi, A. (2017). Ultra-lightweight space arm DELIAN: mechatronic analysis and joint control design. *IFAC-PapersOnLine*, 50(1), 6079–6084.

De Luca, A., Lucibello, P., Ulivi, and G (1989). Inversion techniques for trajectory control of flexible robot arms. *Journal of Robotic Systems*, 6(4), 325–344.

Farruggio, D. and Menini, L. (2000). Two degrees of freedom h_∞ control of a flexible link. In *Proceedings of the 2000 American Control Conference. ACC (IEEE Cat. No. 00CH36334)*, volume 4, 2280–2284. IEEE.

Ferretti, G., Leva, A., and Scaglioni, B. (2014). Object-oriented modelling of general flexible multibody systems. *Mathematical and Computer Modelling of Dynamical Systems*, 20(1), 1–22.

Magnani, G. and Rocco, P. (2010). Mechatronic analysis of a complex transmission chain for performance optimization in a machine tool. *Mechatronics*, 20(1), 85–101.

Malzahn, J. and Bertram, T. (2016). On the equivalence of direct strain feedback and lumped parameter wave echo control for oscillation damping of elastic-link arms. *IEEE Robotics and Automation Letters*, 1(1), 447–454.

O'Connor, W.J., de la Flor, F.R., McKeown, D.J., and Feliu, V. (2009). Wave-based control of non-linear flexible mechanical systems. *Nonlinear Dynamics*, 57(1-2), 113.

Pereira, E., Aphale, S.S., Feliu, V., and Moheimani, S.R. (2010). Integral resonant control for vibration damping and precise tip-positioning of a single-link flexible manipulator. *IEEE/ASME Transactions on Mechatronics*, 16(2), 232–240.

Rusconi, A., Magnani, P., Michaud, S., Gruener, G., Terrien, G., and Merlo, A. (2015). Dextrous lightweight arm for exploration (DELIAN). *Advanced Space Technologies in Robotics and Automation (ASTRA), Noordwijk, The Netherlands.*

Spong, M.W. (1987). Modeling and control of elastic joint robots. *Journal of dynamic systems, measurement, and control*, 109(4), 310–318.

Yang, T.C., Yang, J.C., and Kudva, P. (1992). Load-adaptive control of a single-link flexible manipulator. *IEEE transactions on systems, man, and cybernetics*, 22(1), 85–91.